Resistive Sensors for Smart Objects: Analysis on Printing Techniques

Paolo Bellitti, Michela Borghetti, *Member, IEEE*, Edoardo Cantù, *Graduate Student Member, IEEE*, Emilio Sardini, *Member, IEEE*, and Mauro Serpelloni, *Senior Member, IEEE*

***Abstract*— The growing diffusion and usability of additive printing techniques have created new manufacturing scenarios for products. Printed electronics is playing a key role in the design of next-generation objects. These objects are no longer only able to fulfill their original function, but through specific sensors and circuits can measure physical quantities in the surrounding environment. In this way, a conventional object is made smart, being able to communicate with other objects or remote units. This kind of change fits perfectly into the context of Industry 4.0, where the ability to collect additional information can increase efficiency in the production, transportation, and storage of products. Smart objects can be manufactured with numerous different technologies and materials depending on the performance required and on the specific application. The purpose of this article is to provide an analysis of printed technologies that enable resistive sensors printing on complex surfaces for smart object fabrication. First, an explanation of the technologies under consideration is provided. Then, an analysis of the aspects that affect the final print quality for each technique is provided, highlighting advantages and disadvantages. This article also indicates the limitations and potential of these printed technologies for smart objects.**

***Index Terms*— Aerosol jet printing (AJP), inkjet printing (IJP), laser-induced forward transfer, microdispensing, piezoelectric jetting, plasmadust, printed electronics (PE), resistive sensors, smart objects.**

I. Introduction

THE invention of the first additive manufacturing (AM) technique coincided with the filing of the patent US4575330A: "Apparatus for production of three-dimensional objects by stereolithography" by Hull and Arcadia [1] in 1984. The author describes the lithographic process for the realization of objects starting from their three-dimensional (3-D) model. The technique defined as "AM" involves the realization of an object by overlapping successive sections of it, starting with nothing. It is defined additive as opposed to the classic techniques of subtractive manufacturing, in which starting from a solid block, the desired object is constructed by removing material. In the following decades, AM techniques have been improved and their accessibility is increased [2]–[5].

Manuscript received March 4, 2022; revised May 11, 2022; accepted May 22, 2022. Date of publication June 9, 2022; date of current version June 20, 2022. The Associate Editor coordinating the review process was Dr. Fabricio Guimaraes Baptista. *(Corresponding author: Edoardo Cantù.)*

The authors are with the Department of Information Engineering, University of Brescia, 25123 Brescia, Italy (e-mail: paolo.bellitti@unibs.it; michela.borghetti@unibs.it; e.cantu@unibs.it; emilio.sardini@unibs.it; mauro.serpelloni@unibs.it).

The development and study of new materials suitable or adapted for 3-D deposition allow the fabrication of objects with specific mechanical and electrical properties (4-D printing) [6]. The availability of depositable materials with known electrical properties permits the integration of sensors, electronics, and conductive tracks directly during the production stage of the objects. In this way, it is possible to directly fabricate "smart objects" in which electronics is not simply applied to an existing element, but it is directly embedded in it. "Smart device" or "smart object" is often used to define a generic modern electronic device, revealing a certain ambiguity and confusion about its definition. In [7], a detailed analysis of the scientific literature is carried out with the aim of trying to reduce this ambiguity and define some main characteristic features that an object should have to be defined smart. The three key features defined are: 1) autonomy, intended as the ability to perform an activity or a specific task independently without the need of continuous interaction with the user; 2) connectivity, defined as the possibility of connecting to a network of any type and size with the main purpose of exchanging information with other devices; and 3) context awareness intended as the ability of the device to obtain information about the context to which they belong using specific sensors and also to perform actions independently.

Printed electronics (PE) technologies provide different solutions in the realization of sensors, circuits, antennas, and interconnections directly on the surface of devices to turn any object into a smart one [8]. Low production costs, high variety of materials, and flexibility are only a few examples of advantages provided by PE technologies with respect to conventional electronics production techniques [9], [10]. A remarkable aspect is that different 3-D-PE technologies are emerging, thus permitting us to enter a new design era in which an object can be conceptualized and realized simultaneously in all its parts in a single all-encompassing production step. This last aspect allows to bring a new definition of smart object, i.e., a conventional object preserving its dimensions and purpose, also capable to perceive and measure physical quantities variations, to elaborate and to communicate and/or make autonomous decisions [11]. The availability of data measured in the field environment will allow a deeper testing phase in the application field. Consequently, it will be possible to obtain data directly from the use in the field, enabling assistance of the user and information for the design

TABLE I
TECHNICAL SPECIFICATIONS OF PE TECHNIQUES

Printing Technique	***Inks Viscosity (cP)***	***Minimum Line Width (μm)***	***Layer Thickness (μm)***	***Printing speed (m/min)***	***Axis Configuration***	***Multilayer/multihead***	***Substrates (surface profile and material nature)***	***Ref***
Microdispensing	50-1,000,000	20-300	Dependent on particle size, from 10 nm to 50 μm	Up to 30	3-axis or 5-axis system	Multilayer with Multiple Pass Printing/multihead configuration for the deposition of different materials	Any kind of two-dimensional (2D) and 3D material	[59]–[62]
Inkjet Printing	5-20	30-50	< 0.5-1	15-500	2-axis	Multilayer with Multiple Pass Printing/multihead configuration for the deposition of different materials	Any kind but 2D	[23], [24], [63], [64]
Piezojet	50-200,000	>300	Up to 60	Up to 6	3-axis or 5-axis system	Multilayer with Multiple Pass Printing/multi-head configuration for the deposition of different materials	Any kind of 2D and 3D material	[29], [38], [65]–[67]
Aerosol Jet Printing	UA: 1-5; PA: 1-1,000	~10	0.1-2	Up to 12	3-axis or 5-axis system	Multilayer with Multiple Pass Printing/multi-head configuration for the deposition of different materials	Any kind of 2D and 3D material	[39], [58], [68], [69]
Plasmadust© (Plasma Thermal Spray)	Use of 200 nm 20 μm meshing powders	2-5 mm, up to 200 μm with specific masks applied	Up to 200	Up to 150	3-axis or 5-axis system	Multilayer deposition is possible according to the thermal properties of the previously deposited layers	Metals, glass, ceramics, plastics; both 2D and 3D	[43], [45], [49], [70]
Laser-Induced Forward Transfer	~10 to > 100,000	<20	~0.1	Laser dependent	3-axis	Direct simultaneous multilayer deposition	Any kind of 2D and 3D material	[51], [56], [71]

of new products. At the same time, the smart object is also able to exchange data with nearby devices, and in a more complete view with specific servers, inserting itself in a collaborative scenario in which the attributed function is coordinated and improved remotely by exploiting the realtime monitoring capabilities of the object [12]. Embedded sensing and transmission capabilities are enabling factors both for the classic Internet of Things, oriented to the consumer world, and for the Industrial Internet of Things (IIoT) in which the process is scattered by a network of integrated and connected sensors [13], [14]. Nowadays, the IIoT is not involved in automation control, but it is intended for data collection for supervision or prediction purposes. Big amount of data can permit new predictive maintenance methods also performed with innovative tools such as augmented reality headsets [15], [16].

Smart objects include sensors for sensing the environment, and resistive sensors (force, temperature, or gas sensors) are frequently used for the cost and the ease of fabrication and use [17]. The purpose of this article is to propose, analyze, and discuss the different PE technologies present in the market in order to understand their influences on resistive sensors fabrication, focusing on their performances and process parameters. Section II provides rapid knowledge of the functioning principles of the selected techniques, evidencing which are the characteristic performances of each one. Section III introduces a critical analysis of each parameter evidenced in the previous section, while Section IV presents their possible application areas based on their performance.

II. PRINTING TECHNIQUE'S CHARACTERISTICS

The most used and commercialized PE technologies for the fabrication of resistive sensors directly on the objects are described in this article. All the selected technologies are digital, i.e., they take advantage of computer-aided design (CAD) software to design the printed patterns: no masks are required, and axis movements and the material ejection are controlled according to the digital file. Some technologies [for instance, inkjet printing (**IJP**)] are more suitable for printing on flat surfaces to cover wider areas and thus less for fabricating the sensor on ready-to-use 3-D objects. Other technologies (for instance, Piezojet) are suitable for nonplanar or 3-D surfaces.

The factors characterizing each of the mentioned technologies will be analyzed and summarized in Table I. Specifically,

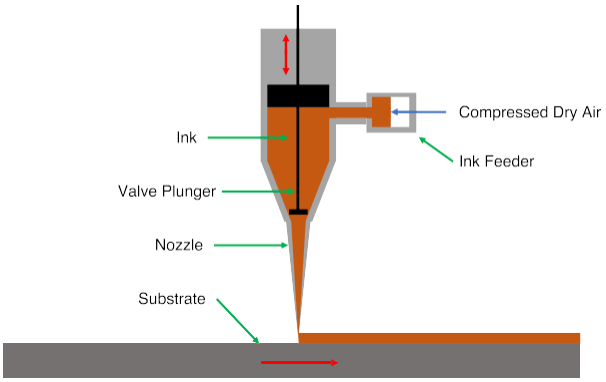

Fig. 1. Microdispensing physical functioning principle.

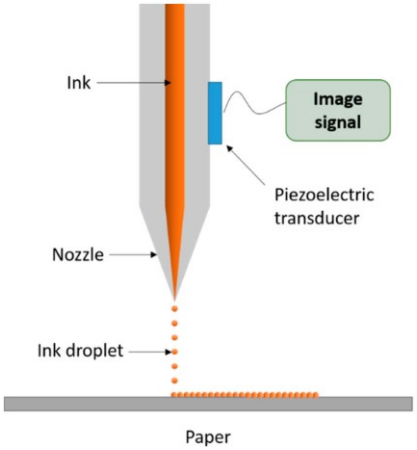

Fig. 2. Inkjet physical functioning principle [26].

these are the following parameters: printing process parameters and setup, ink viscosity and usable materials, geometrical finishes (minimum linewidth and layer thickness), printing process speed, multilayer capabilities, and printing mode. These specifications are essential to select the most proper printing technique for the sensor to be printed on the object. The printing machine apparatus involved in the deposition can also afflict the conclusive performance of the print. One example is the transport losses due to the tubes connecting the spray drying block to the printing head in liquid ink technologies; these losses are related to nonlinearities and tubes that are too long.

A. Microdispensing

Microdispensing is a contact printing technique dispensing the liquid in volumes smaller than a microliter. The system, schematically shown in Fig. 1, consists of a reservoir with a piston driven by compressed air to control the release of material for the pattern deposition. A droplet is formed at the exit of a nozzle and deposited onto the substrate by contact. The diameter of the nozzle determines the geometric characteristics of the deposited drop, while the flow control mechanism determines the volume of the droplet. A solenoid valve or a system of piezoelectric elements is the most used flow control systems. The solenoid valve permits the ejection of the liquid maintained under pressure. The volume of the ejected droplets (between 100 and 1000 nL) is a function of the pressure and the opening time of the solenoid valve [18]. Due to the inertia of the mechanical elements, the time required to obtain the exchange of the valve position is around 1–20 ms [19]. In the flow control by piezoelectric elements, the ejection of the single drop (of 0.5–100-nL volume) is obtained by deforming a thin-walled tube, a capillary wrapped by a piezoelectric element [20]. The reduced inertia of this system permits quick response times of approximately 100 μs.

The cleaning of the capillary is made easier due to the absence of contact between the ejection system and the piezoelectric elements. Due to the pneumatic system, microdispensing can process functional materials even in form of high viscosity ink and pastes. Finally, it is suitable for depositions on 3-D surfaces of various shapes, despite being a contact printing technique [21], [22]. Contact jet dispensing should maintain contact with the substrate, and this reduces the printing speed for preventing surface damages.

B. Inkjet Printing

Inkjet printing (IJP) is currently one of the most widespread and attractive technologies to fabricate PE thanks also to its greater accessibility compared to other techniques [23], [24]. The functional material in a liquid state is transformed into small droplets and deposited onto the substrate. The inkjet printers are divided into two families: continuous inkjet (CIJ) and drop-on-demand (DOD) inkjet printers. In the CIJ printers, the printhead generates, electrically charged, and ejects droplets continuously, while an electric field directs the charged droplet toward the substrate when it is required. The unused droplets are collected in a tank to be reused. In DOD printers, the droplets are generated in the printhead and are forced out from the nozzles when it is required. Droplets can be generated by using two distinct main methods: thermal or piezoelectric. In the thermal DOD, the heat is produced inside the ink chamber for the vaporization of the ink, while in the piezoelectric DOD, a piezoelectric actuator generates the pressure pulse in the fluid to force out the droplets from the nozzle. The piezoelectric DOD (Fig. 2) is the most used because the volume and the speed of the droplet can be better controlled [25].

Electrohydrodynamic jet printing (EHD) is another type of IJP in which a high voltage (0.5–20 kV) is applied between the nozzle and the substrate [25]. The generated electric field causes a droplet ejection when the electrostatic force overcomes the solution surface tension. IJP is considered a contactless printing method, and this prevents cross contamination of the surface, but the distance between nozzle and substrate should be kept under 1 mm. In the IJP process, different parameters influence the obtainable geometrical finishes, like the viscosity according to the geometric characteristics of the nozzle and the distance from the substrate.

C. Piezojet

Piezostack-driven jetting deposition, or Piezojet, belongs to the DOD printing family and allows the deposition of

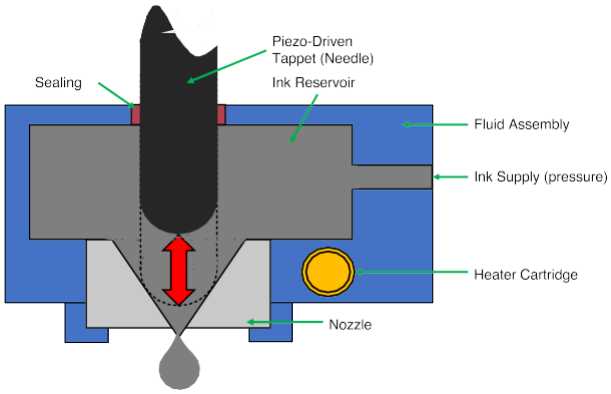

Fig. 3. Piezojet physical functioning principle.

paste and inks from a few to hundreds of thousands of centipoise (<200 000 cP). The droplets are generated and pressed through the nozzle of 50–300 μm diameter by the piezo-driven tappet (needle). The basic mechanism is based on four subsequent stages. Considering Fig. 3, first, at the beginning, the piezoelectric stack is powered ON and the needle and the nozzle are in close contact preventing unwanted ink exit; second, when the signal is generated, the needle raises and separates from the nozzle; third, once the piezoelectric stack is powered OFF, the needle falls in the starting position under an applied electric field; and 4) ink ejection is performed due to the pressure generated during such a movement. This sequence is typically completed in 10 ms [27]–[30]. The reservoir is refilled with new ink contained in an ink supply by a piston, and the heater installed in the proximity of the print head adjusts the viscosity of the functional ink. This aspect is mandatory to enlarge the number of functional materials that can be used, such as screen printing pastes [28], [31]. High jetting frequency is necessary to elaborate high-density/surface tension inks [31] and, in combination with high printing speed, increases the throughput. Great importance has to be addressed to needle–nozzle coupling and nozzle diameter [32]. The nozzle/needle shape (of spherical or conical profiles) should be selected according to the used ink since their shape affects the maximum fluid velocity of the nozzle outlet. The volume of the ejected droplet depends on several parameters. For example, the droplets diameter increases by increasing the opening time of the ejection and the needle displacement (known also as stroke), while the amount of jetted material increases when the needle speed decreases (the outflow time decreases, and the pressure increases). Exceeding the needle speed range where a perfect injection droplet is obtained implies the impossibility to generate droplets or the formation of satellite ones [32], [33]. Needles with a side cap present an additional squeezing effect on the fluid, and the pressure in the cavity and the velocity of the jet are increased, helping to obtain small droplets [34]. Feeding pressure, needle displacement, and working frequency define the volume of the ink in the nozzle orifice to be ejected and the time required for the ink to reach the nozzle [30], [35], [36]. Unlike IJP, Piezojet works at higher nozzle-to-substrate distances due to the high level of the kinetic energy of the droplets and can print on complex and 3-D surfaces without incurring the risk of dispersing functional material in the printing area [37], [38].

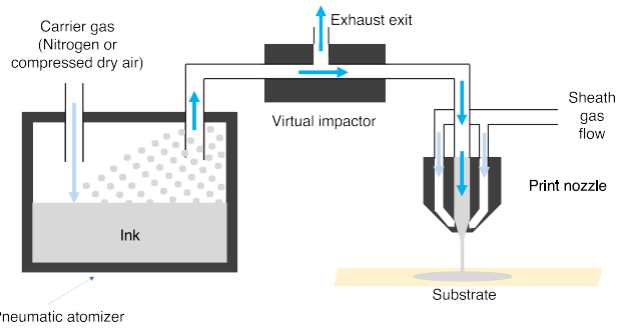

Fig. 4. AJP physical functioning principle.

D. Aerosol Jet Printing

Aerosol jet printing (AJP) is a material jetting AM technique. This technology was developed by Optomec under the Defense Advanced Research Projects Agency (DARPA) Mesoscopic Integrated Conformal Electronics (MICE) program. AJP consists of an aerodynamic focusing process of liquid particles that are accurately deposited onto the substrates placed under the exit nozzle. Four consecutive stages compose the printing process. First, a carrier gas (nitrogen or compressed dry air) transports the aerosol of functional ink generated inside the pneumatic atomizer (PA) or the ultrasonic atomizer (UA). The ink viscosity should be in the range of 1–1000 cP for UA and 1–5 cP for PA. Second, (only for the PA system) due to a virtual impactor placed right after the atomizing block, the superfluous carrier gas is removed, and droplets dimensions adjusted (smaller than 5 μm in diameter). Third, the resulting aerosol is focused inside the print head surrounded by a cylindrical sheath gas flow (one of the process parameters), which prevents possible droplets impacts. The aerosol diameter can be reduced by increasing the sheath gas. Fourth, the whole complex is accelerated entering the printing nozzle, leaves the nozzle, and impacts the substrate, fixed on a moving (and possibly) heated plate, to realize a drying step during printing and/or to evaporate solvents. AJP can be equipped with two different print nozzles: 1) circular nozzle with inner diameters in the range 100–300 μm and 2) wide nozzle with circular (inner diameter of 750 μm) or rectangular orifice (1.5 μm × 2 or 3 mm). The commercially available system prints lines from 10 μm to 3 mm in width and from 100 nm to 10 μm in thickness at translation speeds up to 10–12 mm/s. Fig. 4 represents the deposition phase using AJP [39], [40].

AJP overcomes some of typical printing electronics defects such as nozzles clogging and coffee-ring effects of droplets typical of IJP and Piezojet. One of the strongest AJP advantages is the possibility to selectively print on 3-D complex surfaces [41] and objects with a five-axis configuration. The printing of different materials is possible at the same time with multiple nozzles [42].

E. Plasmadust

Plasmadust technology belongs to the thermal spray family, and it is also known as cold active atmospheric plasma

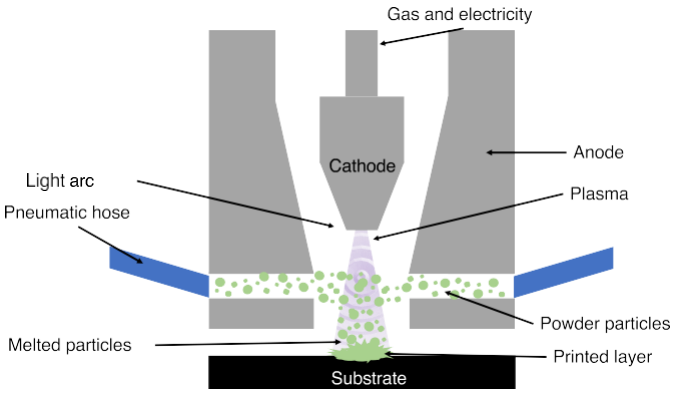

Fig. 5. Plasmadust physical functioning principle.

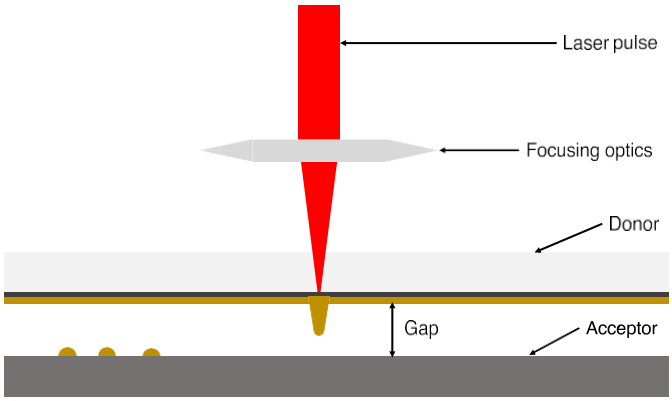

Fig. 6. Laser-induced forward transfer physical functioning principle.

deposition (CAAPD). For example, a direct metallization on thermoplastics can be performed in a one-step process by using this technology. The plasma nozzle is composed of an internal element—the cathode—in which the forming gas fluxes, and an external element—the anode. As schematically shown in Fig. 5, by applying a high-frequency current, a high-energy pulsed arc is generated between cathode and anode, ionizing the process gas (e.g., nitrogen) and transforming it into a low-temperature plasma. In the presence of plasma, the feeding system transports functional powders (200 nm–20 μm in diameter) close to the nozzle and part of the gas energy is transferred to the particles. In such a way, the powders are melted and directed toward the substrate realizing patterns without any use of a solvent to activate the functional material. An exhaustion pipe collects the unused material [43], [44]. In contrast to the other analyzed technologies, plasmadust produces traces with a much greater width (2–5 mm). The width can be reduced by applying a mask on the surface to be coated, but losing the advantage of no postprinting processing [45]–[47]. The thickness and the width are strictly related to powders mesh [48], [49] and the distance between the nozzle and the substrate [46]. If the distance is too shorter, the substrate could present redness and burns due to the high thermal stress; a longer distance could generate focusing problems causing overspray, not well-defined lines, and some areas with not well-plasticized particles.

Plasmadust has several beneficial aspects. First, in contrast to other thermal spray technics, the entire fabrication printing process is realized under atmospheric pressure. Finally, in contrast to other plasma processes, the use of a pulsed plasma implies a lower working temperature (<200 °C), a lower power supply level, and thus lower wear for the nozzle. In this way, even low melting point substrates such as plastics can be used as a substrate [44], [48].

F. Laser-Induced Forward Transfer

In contrast to the previous technologies, laser-induced forward transfer (LIFT) is a direct-write digital printing technology based on laser ablation [50]. As schematically shown in Fig. 6, the functional material is transferred by laser energy source from the donor (a laser-transparent substrate coated with the selected functional material) to the acceptor (the substrate). The pulsed laser beam is generated and focused through specific lenses on the surface of the donor. Depending on the type of functional material deposited and its state, a threshold value at which the donor film starts to deform itself is reached. The irradiated material is accelerated toward the receiver on which it will collapse, depositing the previously heated functional material and forming the desired pattern [51]. Although LIFT is nominally addressed as contactless, the gap between the donor and the acceptor is usually in the microscale, but it could be even millimetric [51], [52]. In some cases, the complete contact of the two substrates generates better printing performances. Despite this, LIFT allows the realization of 3-D complex structures due to a layer-by-layer deposition [53]. In contrast to the other analyzed technologies, LIFT is a solvent-free printing method working in ambient conditions (no high temperature or vacuum chamber required), and this facilitates the process [54]. In addition, LIFT is a nozzle-free printing system so that any kind of clogging problem is avoided. Indeed, the focus here is related to an energy source and not the functional material, which is outside the "working part" of the printing machine [55]. Moreover, no (thermal) post-treatments are required, and therefore, low-temperature substrates, such as paper or plastic, are suitable for LIFT. In LIFT, the functional material is molten and then solidifies once in contact with the receiving substrate. Indeed, the generated droplets have a very low mass, and therefore, despite the high reached temperature when hit by the laser, they do not damage the receiving substrate. LIFT technology works with different kinds of functional materials with a wide viscosity range. Different methods can be used to prepare the donor (spin coating, sputtering, and stencil deposition), and the chosen technique depends on the viscosity of the functional material, which may influence the jetting dynamics [54]. Since LIFT employs a pulsed laser to melt the functional material, a determining factor is the scanning velocity: the higher is the latter, the lower is the bubble time to collapse back to the donor face. This fact leads to possible interferences.

For consecutive jets, high viscous functional materials are recommended [52]. The wide range of viscosity for LIFT is related to the preparation of the donor film before the real printing process. Congruent LIFT or laser decal transfer (LDT)

configuration allows the printing of high viscosity pastes because the printed voxel matches congruently the illuminating laser pulse. The great advantage that comes with this approach is that voxel shape and size become controllable parameters [51], [55], [56].

According to Table I, the maximum printing speed (and therefore throughput) is reached by IJP. Microdispensing, AJP, and Piezojet show similar process speeds because they have been developed for research and development (research and development) applications, in contrast to plasmadust or IJP, which can be naturally scaled for industrial applications. To partially compensate for the limited process speed, LIFT hybrid methods involving roll-to-roll systems have been proposed to increase the supply of functional material, the donor, and realize more traces [53]. The axis configuration defines the movements of the head and the plate on which the object/substrate lies and the possibility to print on 3-D surfaces. For example, in IJP, the object has to be planar since the plate moves in two directions and the distance between the plate and the nozzle is fixed. In the other PE techniques, instead, the head can be moved, as well as the substrate/the object can be moved and rotated according to the printer configuration. In addition, several technologies envisage the installation of several deposition heads in parallel in order to simultaneously print different materials (as in AJP-based systems) or to increase production capacity by using the same material on each printhead [57], [58].

III. Printed Resistance Sensors

In general terms, the resistance of a sensor depends on the resistivity of the sensor material and its geometric dimensions according to the following formula:

$$R = \rho \int_0^l \frac{1}{A(x)}\, dx \tag{1}$$

where R is the electrical resistance expressed in ohm [▲], ρ is the electrical resistivity of the volume of the material into which the current flows expressed in [▲·m], l is the length of the current path [m], and $A(x)$ is the cross section along the x-axis [m^2].

Printing directly the sensor made available some important capabilities. With respect to the traditional sensor, printed sensors can have the following:

1) more flexible geometry;
2) modified resistivity value due to new materials and the sintering process;
3) modified characteristics of the substrate–sensor interface.

Process parameters and the machine setup significantly affect the print quality and, therefore, the geometrical dimension and the resistivity of the printed sensor [60], [72], [73]. Process parameters can be pressures to handle gaseous flows [74] (AJP), plasma intensity and powder feeding (plasmadust), laser intensity (LIFT) [55], [56] pressures to handle valves and pistons (Piezojet), and the type of inert protecting gas and their pressure during printing (AJP, Piezojet, microdispensing, IJP, and plasmadust) [45], [46], [70], [75]. Printing time is another determining factor in the overall quality of the process, and for some technologies, one of the most troubleshooting aspects is the process drift in case of long-term printing sessions, which can generate overspray [76]–[78]. For example, IJP allows maximum printing speed but is affected by nozzle frequent clogging. Conversely, AJP nozzles are clog-resistant, but AJP is a slower printing process and is affected by performance drop. Analytical models have been developed to minimize overspray and increase knowledge of the mechanism and interdependence of involved parameters [79]–[81].

A. Geometry

The main advantage of all the analyzed PE technologies is customization. First, since these technologies are digital, the sensor design is performed via software, and the sensor geometry could be adapted or changed more easily and quickly according to the project specifications. Second, the integration of more printed parts (more sensors, interconnections, and pads) in terms of spatial customization is higher than traditional methods that need the production of all the parts separately on a different substrate.

The accuracy and the cross section $A(x)$ depend on the printed technology specification (minimum width and thickness in Table I). The smaller is $A(x)$, the higher is the resistance. $A(x)$ depends on the width and thickness line. Less is the sensitive area for the sensor, less should be the linewidth, and this is reached by using AJP. For example, in a metallic foil strain gauge, the grid pattern is designed in order to maximize the number of lines subject to strain, and this increases the resistance and the resistance change under strain, as well as decreases the current needed for the measurement. Thin features allow the miniaturization of interconnections and circuits [67], [82], [83]. The minimum layer thickness is reached by using IJP, AJP, and LIFT, but the technology selection depends on the ink (in terms of material and viscosity) and the surface (2-D and 3-D) [84]. However, AJP suffers from less repeatability and reliability of material deposition [85]. The geometrical finishes depend directly on the ink viscosity, and this limits the choice of printing technology.

The larger is the size of the functional material particles, the higher is the viscosity of the ink. Inks with higher viscosity are usually deposited more evenly, the profile of the line tends to form a rectangular shape and the printed line is thicker [86]. The resulting wide section decreases the resistance value, as obtained with microdispensing and Piezojet [38], [67], [87]. Viscous inks and pastes reduce overspray phenomena and allow the exploitation of greater distances between substrate and nozzle for printing on 3-D surfaces. In contrast, such high viscosities limit the realization of fine features.

Furthermore, printing speed affects the line thickness. In the presence of fast processes (e.g., IJP and plasmadust), minor thicknesses would be achieved. Similar considerations can be done considering powder pressure since an increasing powder pressure develops overspray and lower thicknesses. In light of this, more plasma energy is necessary, generating higher thermal stress [45], [49], [75].

B. Resistivity

The ink/paste nature and the curing/sintering process contribute to the final resistance through parameter ρ. The materials differ not only in terms of large families of materials, i.e., conductors and semiconductors, but also in their correspondent bulk material.

1) *Materials*: PE functional materials, in the form of ink or paste, strongly differ from bulk materials. Indeed, PE materials are a combination of functional particles and specific additives, and they can have unique characteristics such as flexibility and stretchability. The most common inks for PE are based on metallic particles and they are used to fabricate interconnections, pads, and the sensitive layers of resistive sensors [45], [53], [64], [67], [88]–[91]. For example, a silver ink contains the specific metal particles (silver in our case) of nano- or micro-particulate size, and this influences the overall viscosity of the material. These particles are found suspended within a medium (solvent) with a specific viscosity and are enveloped by insulating additives and stabilizing agents. The liquid part is composed of organic elements such as additives (to avoid phase separations or particle agglomeration), dispensers (to maintain the appropriate fluidity), and carriers to facilitate the printing process. Higher is the ink viscosity, higher is the solid content, and thus more is the deposited functional material [92]. For example, the solid content of the silver-based inks suitable for IJP and AJP with UA is usually lower than 50 %, while the silver-based ink for AJP with PA can be higher than 70%. Less is the content of functional material and the incidence of micropores inside the printed layer after sintering, the greater is the final resistivity.

Other semiconductors can be used in the fabrication of resistive gas sensors, specifically, metal oxides as in the case of SnO_2, typically used for detecting the presence of gases such as ethanol, methane, and acetone at high operating temperatures [54], [93], [94].

In next-generation printed sensors fabrication scenarios, 2-D materials have been demonstrated to have outstanding physical/chemical properties, which make them highly suitable for optoelectronics, sensors, and energy storage. The most investigated 2-D material is graphene [95]. For example, graphene was used to fabricate a textile strain sensor for detecting human motion and it demonstrated excellent properties in terms of high sensitivity, long-term stability, and great comfort [96]. Recently, a quantization of the electrical resistance has been found in bilayer graphene, irrespective of the material's basic characteristics. In this way, the resistance could be changed with extremely high control irrespective of sensor dimensions [97]. Beyond graphene, other 2-D materials derived from layered bulk 3-D materials, such as carbon nanotube and MXenes, have been found. The term MXene is used to refer to a wide family of materials composed of 2-D layers. Since their discovery, different types of MXenes have been produced and investigated due to their innovative structural, physical, chemical, and sensing properties [98], [99]. The electrical characteristics depend on the functional elements. Using an AJP deposition method in [100], a multifunctional sensor has successfully been fabricated combining graphene and titanium carbide ($Ti_3C_2T_x$) MXene nanoink. The multiple sensing capabilities permit the measurement of strain by evaluating AC impedance and temperature by detecting DC Seebeck voltage. This sensor has an interesting thermopower output (53.6 μV/°C) and high accuracy and stability. Carbon nanotubes are special structures of carbon atoms disposed as a cylinder that can exhibit different conductive behavior according to their spatial arrangement. Carbon nanotube-based inks have been successfully used to develop strain sensors [101], pressure sensors [102], [103], electrochemical and temperature sensors [104], [105], and noncontact gap measuring devices [106]. Excluding LIFT, which follows the laser ablation method, and plasmadust, which belongs to the thermal spray family, other printing techniques work with inks and/or pastes. Microdispensing and Piezojet benefit from a wide viscosity range in which can be found functional materials such as poly(3,4-ethylenedioxythiophene) polystyrene sulfonate (PEDOT:PSS); silver, copper, gallium–indium eutectic (eGaIn) as conductors; carbon, graphene, and carbon nanotubes (both single and multiwall) as resistive materials, $CuO/Cu_2O/Cu$ nanowires and Fe_2O_3/Fe nanospikes as semiconductor, polydimethylsilox-ane (PDMS), and silicones; and adhesives (UV-curable and epoxy glues) as polymeric insulators or strontium titanate (SrTiO3), [28], [66], [67]. AJP, according to the selected atomizer, is suitable for printing a large number of materials such as conductive metals, semiconductors, insulators, various polymers, glues, graphene, carbon nanotubes, and biological material (proteins, enzymes, and glucose) [63], [68], [89], [107]. Even pastes designed for other technologies can be made suitable for AJP due to the use of appropriate solvents [108]. IJP is a rapid and low-cost method to obtain a different kind of sensors [109], by depositing metallic nanoparticle inks (based on gold, silver, and copper) [110], semiconductor inks (such as indium–zinc–tin oxide) [111], and insulators (such as PU-based insulator ink) [112]–[115]. Considering its physical principle, typical plasmadust powders are metallic ones as conductors (Cu-based alloys, CuNi, NiCr, and NiAl), ceramic powders such as NiCrAlY and YSZ, Al_2O_3, $MgAl_2O_4$, or organosilicates for their barrier properties [46], [47], [75], [93], [116]–[118]. As for LIFT, both element materials and complex ones can be used, such as conductive metals (Cu, Al, V, Cr, Ni, and W) or oxides (Al_2O_3, In_2O_3, V_2O_5, and $YBa_2Cu_3O_7$). Also, conductive polymers, composites, and polycrystalline silicon films were studied. The only limitation is in the use of carbon-based or biocompatible materials.

2) *Sintering Process*: After printing, the electrical and mechanical properties of the deposited material are heavily influenced by the sintering process. The sintering process has two phases. In the first phase, the organic additives are evaporated to leave only the functional material. In the second phase, the contribution of thermal energy allows the agglomeration of the particles that, once heated, collapse one on top of the other, thus going to form a network of particles through which the electrons can flow [119]. The sintering process is a critical step in the realization of the

desired patterns because, only with the appropriate heat input, it can achieve the elimination/minimization of voids in the printed material, necessary for the target performances [120], [121]. A low heat input does not allow optimal conduction, while an excessive heat input can lead to burns, ungluing and volumetric cracks along with the selected geometries [122]. In light of this, the inspection (for instance, with X-ray diffractometry) of the internal structure of the printed layer shows the final characteristics, determining the amount of voids present in the volume and the material composition. In [93], the functional layer showed a residual deformation due to a possible mismatch between thermal expansion coefficients between deposited material and substrate, inhomogeneity due to the voids of different sizes (even greater than 50 nm). There are still technical challenges to be overcome that concern the achievement of macroscopically and microscopically void-free structures that can therefore be defined as geometrically uniform and with defined edges. Greater is the printed thickness (as obtained with Piezojet and microdispensing), much time is required for the sintering, and this can increase the thermal stress of the substrate or lead to surface damages [91], [123]. LIFT and plasmadust do not need sintering postprocess but burns or damages can occur during the material deposition.

C. Substrate–Sensor Interface

The compatibility between substrate and ink affects the behavior of the sensor. When using porous substrates such as paper, for example, the ink penetrates the cellulose layer. This effect depends on the properties both of the ink and the substrate porosity. In some cases, the porosity of the substrate has been exploited to fabricate the sensor. Paper substrate functionalized by the ink has allowed the measurement of gaseous samples to detect the presence of ammonia in humid environments, discriminating different concentrations [124], and deformations due to sensors based on cellulose substrate [125], [126].

Surface preparation is crucial; surface roughness influences the adhesion to the substrate and also cleaning operations are usually requested. In the LIFT case, donor preparation is one of the most delicate steps influencing the final results of the printed sensor. In the case of laser-sensitive materials, a coating must be performed with a sacrificial layer, the dynamic release layer (DRL). The DRL is placed between donor film and donor substrate to absorb the greatest part of the laser radiation and to provide the thrust to accelerate a fraction of the donor toward the receiving substrate. Metal layers and triazene polymers are typically used for such a purpose [51], [127].

The use of flexible polymer films, such as Kapton, is widespread in PE, and a similar argument applies to flexible 3-D objects. The compatibility between these materials and various functional inks must be evaluated appropriately. The various microscopy techniques come in help in this sense, allowing to determine the possible presence of cracks or fractures along the path of the stapled patterns. The presence of small cracks leads to a change in the section useful for the transport of electrons, thus raising, in general, the electrical resistance. In the worst cases, complete pattern breakage can be achieved. This is one of the reasons why normally in the chemical composition of the inks are found polymers that facilitate not only the adhesion but also allow to have more flexibility from the printed traces [128], [129]. For applications with stretchability requirements—such as smart clothing—stretchable inks are demanded to follow the deformation of the substrate without seeing a change in their properties [130], [131]. In the flexible electronics field, studies have been carried out on the use of inkjet technology in transparent thin-film transistors (TFTs) realization [132].

Furthermore, the deposition of resistive sensors through digital printing techniques allows a high level of integration of the sensitive element directly on the functionalized object difficult to obtain through traditional application techniques. For example, in strain gauge applications, commercial sensors are generally applied to the target surfaces through specific glues interposed between the sensor substrate and the object surface. The glue interposition adds a layer that contributes to the overall sensitivity reduction. In addition, the ensemble substrate glue can increase the sensor settle time due to a phenomenon called creep related to materials elasticity. Since there is no intermediate layer between the object surface and the sensitive element, it is possible to obtain a more direct measure of the surface deformation. Similarly, temperature sensors are generally encapsulated in ceramic protective enclosures which, although specially designed, could introduce thermal inertia and could reduce the response time of the sensor. Direct deposition permits overcoming these limitations: the printed materials adhere directly to the substrate. Since there is no need for glues forming intermediate layers, it is possible to obtain greater performance.

Another key factor in selecting the proper technology to realize a resistive sensor for a smart object is the possibility to perform a multilayer deposition (insulating layer, sensitive layer, and conductive traces). In most cases, multilayer deposition always needs a dedicated design for the whole device, although the different layers/parts are fabricated at different moments. Markers are typically used to align the layers and facilitate this operation in IJP, AJP, microdispensing, and piezojet. For example, AJP and Piezojet, native for depositions on complex and 3-D surfaces, are equipped with camera systems for alignment with specific markers. Therefore, AJP is equipped with a system that guarantees an alignment accuracy of $\pm 6\ \mu$m [68], [107]. Piezojet, on the other hand, guarantees the repeatability of $\pm 10\ \mu$m [28]. The multilayer deposition is more critical in plasmadust in terms of thermal impact and substrate-material functional coupling since it is based on the plasticization of powder particles by plasma. This is also to avoid damage to the underlying functional layers. With LIFT, it is possible to realize simultaneous multilayer deposition due to the movement of the donors that can be of different origins, especially when implementing roll-to-roll systems that can facilitate the manufacturing process. In reality, multiple deposition of the same material is needed for homogeneous traces because discontinuities and swellings can be found

along the traces due to the deformations induced in the donor by the previous depositions [53], [55].

IV. Applications: RTD, Strain, and Gas Sensors

Among the various categories of resistive sensors, three popular families were analyzed: resistance temperature detectors (RTDs), strain gauges, and gas sensors. The first two families are widely used both for their simplicity of implementation and for the ease with which the output signal is managed and conditioned. The latter represents a promising field in which encouraging results have been obtained with 3-D printing fabrication techniques.

A. RTD Sensors

One of the main resistive sensor categories is represented by RTDs. In this case, the change in resistance occurs mainly due to the dependence between the resistivity of the material (ρ) and the temperature, in the first approximation, rather than from the variation of the geometric sizes. For metals, a linear relationship exists and binds resistivity to temperature according to the following formula:

$$\rho(T) = \rho_{T_0}[1 + \alpha(T - T_0)] \tag{2}$$

where T_0 is the reference temperature and ρ_{T_0} is the resistivity at T_0. For example, for stainless steel $\rho_{0\,^\circ C} = 6.9\times10^{-7}$ Ω·m, α is the resistance temperature coefficient, T is the temperature of the resistive sensor, and $\rho(T)$ is the resistivity at temperature T.

The most used RTDs are those where the conductive filament is formed by platinum, nickel, or copper [75], [128], [133]–[135]. This filament is deposited on a substrate, generally ceramic, for its good thermal conduction characteristics. The filaments are calibrated so that at 0 °C, a standard resistance defined as R_0 is obtained. Common sensors that exploit this property are the commercially named Pt100 and Pt1000, elements composed of platinum and calibrated so that their resistance is, respectively, 100 and 1000 Ω at 0 °C.

Metal oxides can also be successfully used in the production of temperature sensors, as in the case of a NiO thermistor printed directly on the cutting tool insert. A custom formulation was made for the above ink, printed via AJP through UA, to which two silver ink printed terminations were added. The sensor operated over a range of 30 °C–250 °C without hysteretic effects showing a high-temperature sensitivity with a B constant of about 4310 K, following the Arrhenius equation. B constant represents the ratio between the activation energy due to temperature in resistive processes and Boltzmann's constant. Also, the response time of the printed thermistors was almost as fast as that of the feedback thermocouple. This can be seen as a typical example of the application of printed sensors in a harsh environment due to the combined presence of temperature and shear stresses due to cutting operations [136].

Considering instead of conventional conductive materials, temperature sensors can be realized with the usage of both alloy formulation inks or pure metal inks. The first case can be well represented by the realization of flexible temperature sensors due to a Cu–CuNi ink. AJP process for the deposition of the metallic nanoparticles ink was followed by laser sintering at the low powers of 100 and 400 mW under a shroud of inert gas to minimize oxidation. First, the sensors were studied in terms of microstructure composition due to scanning electron microscopy, X-ray photoemission spectroscopy, transmission electron microscopy, and selective area electron diffraction. The functional layer is the result of fused nanoparticles with porosities ranging from 9% to 24% through the thickness of the films. An oxide phase was detected for Cu films, not affecting the sensor performance after repeated tests up to a temperature of 140 °C. The sensor performance appeared to be independent of the manufacturing conditions of the AJP process, showing a highly linear response as a function of the temperature and the highest sensitivity among film-based sensors yet reported in the literature. Flexibility tests showed a stable device performance after 200 bending cycles at three different radii and 200 twisting cycles [137].

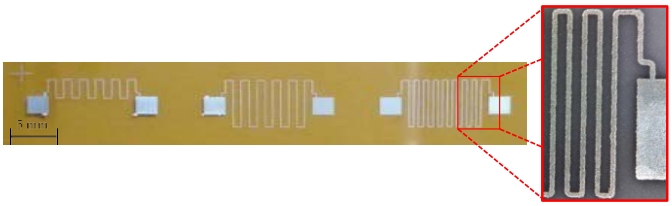

Fig. 7. Example of printed RTD on a Kapton film [12].

Once again, the particularity of the formulation of the inks used leads to a strong dependence on the result. For example, RTDs have been realized by AJP using an ink with a high rate of silver nanoparticulate (over 95%) to obtain sensors that allow the measurement of temperature up to 400 °C–450 °C. This is the reason why the sensors were spray-coated with a specific protecting layer able to resist until 450 °C. A first test regarded the adhesion and was realized by an adhesion tape test. With the purpose to define the α coefficient of the sensors, they were characterized in a controlled temperature oven in the range 35 °C–140 °C, considering a Pt100 as feedback. The overall α coefficient was measured and resulted as 0.00315 K^{-1}, slightly lower than bulk silver (α = 0.00380 K^{-1}) and the one of Pt100 feedback (α = 0.00385 K^{-1}) [12]. Fig. 7 presents a prototype of RTD printed on a Kapton film using a silver ink.

B. Strain Sensors

Strain sensors are devices used to measure strain on an object. They are generally composed of a conductive element, usually a grid with a repetitive pattern, placed on a deformable substrate. A deformation of the substrate causes a change in the size of the sensitive elements, which varies its resistance. The application of these sensors to mechanically characterized objects also permits measuring forces, pressures, tension, or weights. The use of silver-based inks with specific formulations to be deposited on different types of substrates is widespread. Some formulations include specific additives for

the production of sensors on polymeric or paper substrates. With this ink, for example, strain sensors have been made directly on plastic tubes, obtaining a gauge factor (GF) of 2.55 and a thermal resistance coefficient of 150 ppm/°C in the range 0 °C–40 °C (humidity 15% ± 2%), the half of bulk silver [138]. The use of PE also allows the realization of next-generation systems with unconventional geometries as in the case of wearable and flexible devices [100]. One possibility concerns the realization of a custom wearable device for stretch measurement. It is about a skin-like stretch sensor capable to measure in the presence of highly stretched regions like around joint areas. Due to the nonuniform auxetic deformation behavior of the skin around those spots, it is mandatory that the electronics presents the same Poisson's ratio (PR) distribution. Due to the combination of Polyjet and Piezojet, a re-entrant honeycomb structure was chosen to obtain tunable PR, by changing the interior angle of each unit cell. In such a way, it is possible to map the PR for each unit cell to know the deformation of the covered skin because the obtained structure would have the same mechanical property and deformation behavior. In light of this, the shear stress at the connection areas between wearable electronics and human skin was limited, an impossible achievement for conventional configurations, which would surely increase the attachment stability and give flexibility and comfort to a possible patient [139]. Another case of a low-cost wearable flexible and stretchable strain sensor, applicable in sectors such as home healthcare and wearable devices, was developed due to AJP. Here, the dependence of silver characteristics, performance, and microstructure as a function of laser sintering parameters was investigated, in order to achieve their optimization. The results showed that the sensor is lightweight, flexible, and stretchable and has good sensitivity and stability for 700 cycles of repeated bending, being capable to detect large, induced strains [91]. Strain sensors have also been successfully made using organic materials such as poly(3,4-ethylenedioxythiophene):poly(styrene sulfonate) (PEDOT:PSS), a conductive polymer. In this application, in order to ensure proper adhesion between the chosen materials (silver ink and polyimide sheet as substrate), it was necessary to treat the polyimide with a plasma treatment. Crosshatch ink adhesion tape test confirmed the effectiveness of the plasma treatment. The strain–resistance curve was determined due to an electromechanical dynamometer, inducing a uniaxial deformation parallel to the length direction of the sensor. The strain–resistance behavior was not linear but could be approximated by a second-order line. With respect to silver-based strain gauges, the sensitivity and the strain limit of the PEDOT: PSS-based sensors are higher due to their electrical and mechanical properties [140]. Inkjet technology has been successfully used to fabricate strain sensors. As mentioned, this printing technique is suitable for low-cost rapid prototyping. In [141], strain gauge sensors were manufactured by depositing silver-based inks (with different silver contents) on a flexible PET (polyethylene terephthalate) substrate using both desktop and professional inkjet printers. Results show good transducing (GF between 1.07 and 2.03) and stability characteristics.

C. Gas Sensors

Gas sensors are devices capable of detecting or quantifying the presence of a target gas in the environment. The most common transduction principles are based on optical, electrochemical, or semiconductor proprieties.

Semiconductor-based gas sensors are generally composed of tin or tungsten oxide film combined with catalysts or dopants. When the sensitive film is exposed to the target gas it reacts, charged ions are released and the film resistance changes.

Resistive gas sensors can be successfully manufactured using semiconductor materials, such as metal oxides as in the case of SnO_2. LIFT technology was employed in the realization of gas sensors, starting from different SnO_2-coated donor substrates without DRL. Different transfer conditions were studied, evidencing that sputtered and nanoparticle layers were not satisfactory. A new approach to decomposing the transfer material during LIFT transfer was developed. Tests with ethanol, acetone, and methanol as analytes were carried out, showing a large resistance drop for all three tested substances, thus proving the feasibility of using LIFT to print SnO_2 based on different precursor materials for sensing applications [54].

Plasmadust was a useful alternative in producing SnO_2 gas sensors on alumina substrates and then characterized by scanning electron microscopy and X-ray diffraction. Functional layers were realized by varying the plasma forming gas composition, i.e., nitrogen with and without hydrogen. Ethanol sensing tests were performed in a quasi-static chamber at 175 °C–300 °C. The coating manufactured without hydrogen showed a higher response in ethanol present in the range of 25–300 ppm. The coating exhibited excellent repeatability characteristics in the presence of ethanol at 300 °C. Relative humidity tests, temperature influence, and cross sensitivity with acetone and isopropanol were also carried out [93].

Hydrogen sensing is very important because of its peculiar properties like being colorless, odorless, and highly explosive gas. SnO_2 layers were successfully deposited on alumina substrates for such a purpose. A dynamic gas sensing chamber was used during tests, in the presence of 500 ppm of H_2, SnO_2 coating exhibited 80% response at 250 °C with a response time of 30 s and repeatability of sensing characteristics over a prolonged duration. For steam reforming of ethanol, its decomposition on the metal surface leads to the formation of CH_4 and CO as well. In light of this, the sensors were studied in presence of these compounds, evidencing that the functional SnO_2 coating was cross sensitive to CO and CH_4 [94].

Ammonia and its compounds are toxic to the human body being responsible for severe pathologies (from migraine and allergies to carcinogenesis). To detect their presence inside food packaging due to the meat or fish degradation, a paper-based gas sensor was developed. Due to the intrinsic hygroscopic characteristics of paper, cellulose fibers contain moisture as a consequence of absorption from the surrounding environment, which promotes the electrical detection of water-soluble gases such as ammonia. Carbon interdigitated electrodes were AJ printed and flash lamp annealed on chromatographic paper. The sensors were tested at different relative

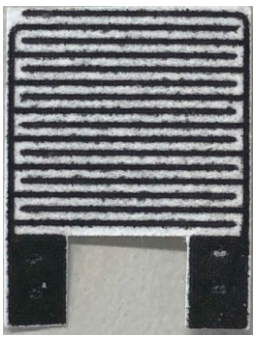

Fig. 8. Example of a paper-based resistive gas sensor.

humidity (RH) values (75%, 80%, 90%, and 100%) and in presence of different ammonia concentrations (3, 6, 9, and 12 ppm). A proportional decrease of resistance was evidenced in increasing RH. As for ammonia detection, the sensors showed a resistance decrease of 15% in the presence of the lowest concentration of 3 ppm [124]. Fig. 8 presents the first concept of a paper-based resistive gas sensor printed on chromatographic paper using carbon ink.

V. Conclusion

This article captures an overview of the capabilities of printed resistive sensors to measure physical or chemical quantities in present and future scenarios. The innovative use of printed technologies could help in the near future in the development of smart objects, able to perceive their original functionality, measure, and communicate. Having different physical characteristics, these technologies have the capability to encounter different required performance that fits well for devoted applications. In light of this, their characteristics have been investigated, to distinguish their functioning principles, usability, applications, and limits. Inside a collaborative scenario, these new smart objects will be able, both in our daily lives and in working/production context, to provide useful information to users to make current decisions and, thanks to communication with devoted servers, to perform autonomous decisions.

At the same time, this sector still needs research to achieve the greatest possible diffusion and fully exploit the possibilities offered by these new methodologies. The design phase of the patterns to be printed requires attention to the placement of certain geometric elements according to the type of substrate in use. In addition, the determination of the process parameters for printing is a delicate and laborious phase since it is necessary to realize custom processes dedicated to a specific combination of materials. The result of this step influences not only the final electrical and geometrical properties of the printed element but also the printing process itself. Indeed, once properly defined, the optimal process parameters allow the printing of several elements consecutively without interruptions for cleaning and avoiding process drifts and overspray. The latter phenomena are defects of the printing process that lead to an inevitable downtime for cleaning.

With a view to future increased deployment of these innovative technologies for making sensors and smart objects, more attention should also be directed to the design and study of complex 3-D patterns. This fact can lead to the evaluation of the fabrication limits of the proposed methods, suggesting new solutions to implement such an approach in other application fields enabling large production volumes and moving ever more decisively into the era of smart objects.

References

[1] C. W. Hull and C. Arcadia, "Apparatus for production of three dimensional objects by stereolithography," U.S. Patent 6 027 324-A, 1984. Accessed: Oct. 16, 2021.

[2] A. Rindfleisch, M. O'Hern, and V. Sachdev, "The digital revolution, 3D printing, and innovation as data," *J. Product Innov. Manage.*, vol. 34, no. 5, pp. 681–690, Sep. 2017.

[3] G. Allevi *et al.*, "Investigating additive manufactured lattice structures: A multi-instrument approach," *IEEE Trans. Instrum. Meas.*, vol. 69, no. 5, pp. 2459–2467, May 2020.

[4] M. Norouzi, D. C. Saha, H. Jahed, and N. Masoumi, "A phase variation-based smart structure for crack detection on metals using cold spray additive manufacturing," *IEEE Trans. Instrum. Meas.*, early access, Dec. 6, 2021, doi: 10.1109/TIM.2021.3132994.

[5] N. J. Goddard and R. Gupta, "3-D printed analytical platform for automation of fluid manipulation applied to leaky waveguide biosensors," *IEEE Trans. Instrum. Meas.*, vol. 70, pp. 1–12, 2021.

[6] F. Momeni, S. M. N. M. Hassani, X. Liu, and J. Ni, "A review of 4D printing," *Mater. Des.*, vol. 122, pp. 42–79, May 2017.

[7] M. Silverio-Fernández, S. Renukappa, and S. Suresh, "What is a smart device?—A conceptualisation within the paradigm of the Internet of Things," *Visualizat. Eng.*, vol. 6, no. 1, pp. 1–10, May 2018.

[8] S. Cruz, D. Dias, J. C. Viana, and L. A. Rocha, "Inkjet printed pressure sensing platform for postural imbalance monitoring," *IEEE Trans. Instrum. Meas.*, vol. 64, no. 10, pp. 2813–2820, Oct. 2015.

[9] K.-S. Kwon, M. K. Rahman, T. H. Phung, S. Hoath, S. Jeong, and J. S. Kim, "Review of digital printing technologies for electronic materials," *Flexible Printed Electron.*, vol. 5, no. 4, p. 43003, Nov. 2020.

[10] R. Rayhana, G. G. Xiao, and Z. Liu, "Printed sensor technologies for monitoring applications in smart farming: A review," *IEEE Trans. Instrum. Meas.*, vol. 70, pp. 1–19, 2021.

[11] G. Kortuem, F. Kawsar, V. Sundramoorthy, and D. Fitton, "Smart objects as building blocks for the Internet of Things," *IEEE Internet Comput.*, vol. 14, no. 1, pp. 44–51, Jan. 2010.

[12] M. Borghetti, E. Cantù, E. Sardini, and M. Serpelloni, "Future sensors for smart objects by printing technologies in industry 4.0 scenario," *Energies*, vol. 13, no. 22, p. 5916, Nov. 2020.

[13] P. Ferrari, A. Flammini, E. Sisinni, S. Rinaldi, D. Brandão, and M. S. Rocha, "Delay estimation of industrial IoT applications based on messaging protocols," *IEEE Trans. Instrum. Meas.*, vol. 67, no. 9, pp. 2188–2199, Sep. 2018.

[14] G. D. Renzone, E. Landi, M. Mugnaini, L. Parri, G. Peruzzi, and A. Pozzebon, "Assessment of LoRaWAN transmission systems under temperature and humidity, gas, and vibration aging effects within IIoT contexts," *IEEE Trans. Instrum. Meas.*, vol. 71, pp. 1–11, 2021.

[15] L. Angrisani, P. Arpaia, A. Esposito, and N. Moccaldi, "A wearable brain–computer interface instrument for augmented reality-based inspection in industry 4.0," *IEEE Trans. Instrum. Meas.*, vol. 69, no. 4, pp. 1530–1539, Apr. 2020.

[16] P. Arpaia, N. Moccaldi, R. Prevete, I. Sannino, and A. Tedesco, "A wearable EEG instrument for real-time frontal asymmetry monitoring in worker stress analysis," *IEEE Trans. Instrum. Meas.*, vol. 69, no. 10, pp. 8335–8343, Oct. 2020.

[17] H.-L. Wei, P. Kumar, and D.-J. Yao, "Printed resistive sensor array combined with a flexible substrate for ethanol and methane detection," *ECS J. Solid State Sci. Technol.*, vol. 9, no. 11, Jul. 2020, Art. no. 115008.

[18] W. D. Niles and P. J. Coassin, "Piezo- and solenoid valve-based liquid dispensing for miniaturized assays," *ASSAY Drug Develop. Technol.*, vol. 3, no. 2, pp. 189–202, Apr. 2005.

[19] S. Bammesberger *et al.*, "A low-cost, normally closed, solenoid valve for non-contact dispensing in the sub-μL range," *Micromachines*, vol. 4, no. 1, pp. 9–21, Feb. 2013.

[20] J. Friend and L. Yeo, "Piezoelectric Microdispenser," *Encycl. Microfluid. Nanofluidics*, D. Li, Ed. Boston, MA, USA: Springer, 2008, pp. 63–86. [Online]. Available: https://link.springer.com/referenceworkentry/10.1007/978-0-387-48998-8_1243#howtocite, doi: 10.1007/978-0-387-48998-8_1243.

[21] E. A. Rojas-Nastrucci, A. D. Snider, and T. M. Weller, "Propagation characteristics and modeling of meshed ground coplanar waveguide," *IEEE Trans. Microw. Theory Techn.*, vol. 64, no. 11, pp. 3460–3468, Nov. 2016.

[22] U. R. Dominguez, "3D printed impedance elements by microdispensing," ETD Collect. Univ. Texas, El Paso, TX, USA, Tech. Rep. AAI1540954, 2013. Accessed: Oct. 16, 2021. [Online]. Available: https://scholarworks.utep.edu/dissertations/AAI1540954

[23] A. Al-Halhouli, H. Qitouqa, A. Alashqar, and J. Abu-Khalaf, "Inkjet printing for the fabrication of flexible/stretchable wearable electronic devices and sensors," *Sensor Rev.*, vol. 38, no. 4, pp. 438–452, Jan. 2018.

[24] Y. Guo, H. S. Patanwala, B. Bognet, and A. W. K. Ma, "Inkjet and inkjet-based 3D printing: Connecting fluid properties and printing performance," *Rapid Prototyping J.*, vol. 23, no. 3, pp. 562–576, Apr. 2017.

[25] H. Gudapati, M. Dey, and I. Ozbolat, "A comprehensive review on droplet-based bioprinting: Past, present and future," *Biomaterials*, vol. 102, pp. 20–42, Sep. 2016.

[26] J. Long, A. Nand, and S. Ray, "Application of spectroscopy in additive manufacturing," *Materials*, vol. 14, no. 1, p. 203, Jan. 2021.

[27] J. Sohn and S.-B. Choi, "Identification of operating parameters most strongly influencing the jetting performance in a piezoelectric actuator-driven dispenser," *Appl. Sci.*, vol. 8, no. 2, p. 243, Feb. 2018.

[28] M. Mueller and J. Franke, "Feasability study of piezo jet printed silver ink structures for interconnection and condition monitoring of power electronics components," in *Proc. IEEE 19th Electron. Packag. Technol. Conf. (EPTC)*, Dec. 2017, pp. 1–5.

[29] M. Ankenbrand, Y. Eiche, and J. Franke, "Programming and evaluation of a multi-axis/multi-process manufacturing system for mechatronic integrated devices," *Proc. Int. Conf. Electron. Packag. (ICEP)*, 2019, pp. 273–278, doi: 10.23919/ICEP.2019.8733548.

[30] S. Lu, G. Cao, H. Zheng, D. Li, M. Shi, and J. Qi, "Simulation and experiment on droplet formation and separation for needle-type micro-liquid jetting dispenser," *Micromachines*, vol. 9, no. 7, p. 330, Jun. 2018.

[31] J. W. Sohn, J. Jeon, M. Choi, and S.-B. Choi, "Critical operating factors of a jetting dispenser driven by piezostack actuators: Statistical analysis of experimental results," *J. Adhes. Sci. Technol.*, vol. 32, no. 4, pp. 359–374, Feb. 2018.

[32] X. Huang *et al.*, "Research on nozzle and needle combination for high frequency piezostack-driven dispenser," *Int. J. Adhes. Adhesives*, vol. 96, Jan. 2020, Art. no. 102453.

[33] Y. Yang *et al.*, "Influence of needle impact velocity on the jetting effect of a piezoelectric needle-collision jetting dispenser," *AIP Adv.*, vol. 9, no. 4, Apr. 2019, Art. no. 045302.

[34] X. Huang *et al.*, "Effect of enhanced squeezing needle structure on the jetting performance of a piezostack-driven dispenser," *Micromachines*, vol. 10, no. 12, p. 850, Dec. 2019.

[35] S. Lu, X. Chen, H. Zheng, Y. Zhao, and Y. Long, "Simulation and experiment on droplet volume for the needle-type piezoelectric jetting dispenser," *Micromachines*, vol. 10, no. 9, p. 623, Sep. 2019.

[36] M. A. Trimzi, Y. B. Ham, B. C. An, Y. M. Choi, J. H. Park, and S. N. Yun, "Development of a piezo-driven liquid jet dispenser with hinge-lever amplification mechanism," *Micromachines*, vol. 11, no. 2, p. 117, Jan. 2020.

[37] Q. H. Nguyen, J. C. Jeon, and S.-B. Choi, "Optimal design of a jetting dispenser actuated by a dual piezoactuator," *Proc. SPIE*, vol. 9057, Mar. 2014, Art. no. 90572U.

[38] R. Zhang, V. Kolbin, M. Süttenbach, M. Hedges, and O. Amft, "Evaluation of 3D-printed conductive lines and EMG electrodes on smart eyeglasses frames," in *Proc. ACM Int. Symp. Wearable Comput.*, Oct. 2018, pp. 234–235.

[39] S. Binder, M. Glatthaar, and E. Rädlein, "Analytical investigation of aerosol jet printing," *Aerosol Sci. Technol.*, vol. 48, no. 9, pp. 924–929, Sep. 2014.

[40] H. W. Tan, T. Tran, and C. K. Chua, "A review of printed passive electronic components through fully additive manufacturing methods," *Virtual Phys. Prototyping*, vol. 11, no. 4, pp. 271–288, Oct. 2016.

[41] E. Cantu *et al.*, "Printed multi-EMG electrodes on the 3D surface of an orthosis for rehabilitation: A feasibility study," *IEEE Sensors J.*, vol. 21, no. 13, pp. 14407–14417, Jul. 2021.

[42] H. Yang, M. T. Rahman, D. Du, R. Panat, and Y. Lin, "3-D printed adjustable microelectrode arrays for electrochemical sensing and biosensing," *Sens. Actuators B, Chem.*, vol. 230, pp. 600–606, Jul. 2016.

[43] R. Schramm and J. Franke, "Electrical functionalization of thermoplastic materials by cold active atmospheric plasma technology," in *Proc. IEEE 15th Electron. Packag. Technol. Conf. (EPTC)*, Dec. 2013, pp. 108–113.

[44] *MesoScribeTM | MesoPlasmaTM Printed Electronics*. Accessed: Oct. 16, 2021. [Online]. Available: https://www.mesoscribe.com/

[45] R. Schramm, J. Hörber, C. Dold, and J. Franke, "Electrical functionalization of thermoplastics by combining plasmadust coating and aerosol jet printing," *Adv. Mater. Res.*, vol. 1038, pp. 43–48, Sep. 2014.

[46] D. Korzec and S. Nettesheim, "Application of a pulsed atmospheric arc plasma jet for low-density polyethylene coating," *Plasma Processes Polym.*, vol. 17, no. 1, Jan. 2020, Art. no. 1900098.

[47] J. Longtin, S. Sampath, S. Tankiewicz, R. J. Gambino, and R. J. Greenlaw, "Sensors for harsh environments by direct-write thermal spray," *IEEE Sensors J.*, vol. 4, no. 1, pp. 118–121, Feb. 2004.

[48] D. Tejero-Martin, M. Rezvani Rad, A. McDonald, and T. Hussain, "Beyond traditional coatings: A review on thermal-sprayed functional and smart coatings," *J. Thermal Spray Technol.*, vol. 28, no. 4, pp. 598–644, Apr. 2019.

[49] J. Franke, A. Syed-Khaja, R. Schramm, and R. Ochs, "Investigations in the optimization of power electronics packaging through additive plasma technology," *Proc. CIRP*, vol. 37, pp. 59–64, Jan. 2015.

[50] G. Hennig, "Lasersonic LIFT process for large area digital printing," *J. Laser Micro/Nanoeng.*, vol. 7, no. 3, pp. 299–305, Nov. 2012.

[51] P. Serra and A. Pique, "Laser-induced forward transfer: Fundamentals and applications," *Adv. Mater. Technol.*, vol. 4, no. 1, pp. 1–33, 2019.

[52] D. Tsakona, I. Theodorakos, A. Kalaitzis, and I. Zergioti, "Investigation on high speed laser printing of silver nanoparticle inks on flexible substrates," *Appl. Surf. Sci.*, vol. 513, May 2020, Art. no. 145912.

[53] S. Cohen, O. Ermak, I. Peled, and Z. Kotler, "High throughput LIFT printing of electric circuitry," *Proc. SPIE*, vol. 11271, Mar. 2020, Art. no. 112710C.

[54] T. Mattle, A. Hintennach, T. Lippert, and A. Wokaun, "Laser induced forward transfer of SnO_2 for sensing applications using different precursors systems," *Appl. Phys. A, Solids Surf.*, vol. 110, no. 2, pp. 309–316, Feb. 2013.

[55] P. Sopeña, J. M. Fernández-Pradas, and P. Serra, "Laser-induced forward transfer of conductive screen-printing inks," *Appl. Surf. Sci.*, vol. 507, Mar. 2020, Art. no. 145047.

[56] M. Jalaal, M. Klein Schaarsberg, C.-W. Visser, and D. Lohse, "Laser-induced forward transfer of viscoplastic fluids," *J. Fluid Mech.*, vol. 880, pp. 497–513, Dec. 2019.

[57] J. Machiels, A. Verma, R. Appeltans, M. Buntinx, E. Ferraris, and W. Deferme, "Printed electronics (PE) as an enabling technology to realize flexible mass customized smart applications," *Proc. CIRP*, vol. 96, pp. 115–120, Jan. 2021.

[58] A. Chletsou, C. Crump, J. Papapolymerou, and J. F. Locke, "Aerosol jet printed antenna for vehicular communications," in *Proc. Antenna Meas. Techn. Assoc. Symp. (AMTA)*, Nov. 2020, pp. 1–4.

[59] J. Sun, J. H. Ng, Y. H. Fuh, Y. S. Wong, H. T. Loh, and Q. Xu, "Comparison of micro-dispensing performance between microvalve and piezoelectric printhead," *Microsyst. Technol.*, vol. 15, no. 9, pp. 1437–1448, Sep. 2009.

[60] G. Percin and B. T. Khuri-Yakub, "Piezoelectrically actuated flextensional micromachined ultrasound droplet ejectors," *IEEE Trans. Ultrason., Ferroelectr., Freq. Control*, vol. 49, no. 6, pp. 756–766, Jun. 2002.

[61] G. T. Carranza, U. Robles, C. L. Valle, J. J. Gutierrez, and R. C. Rumpf, "Design and hybrid additive manufacturing of 3-D/volumetric electrical circuits," *IEEE Trans. Compon., Packag., Manuf. Technol.*, vol. 9, no. 6, pp. 1176–1183, Jun. 2019.

[62] S. Sikulskyi, S. L. Yu, E. A. Rojas-Nastrucci, J. Park, and D. Kim, "Soft and printable electrodes for flexible elastomer actuators," in *Proc. Electroactive Polym. Actuat. Devices (EAPAD) XXII*, May 2020, p. 59.

[63] N. Saengchairat, T. Tran, and C.-K. Chua, "A review: Additive manufacturing for active electronic components," *Virtual Phys. Prototyping*, vol. 12, no. 1, pp. 31–46, 2017.

[64] M. Borghetti, E. Sardini, and M. Serpelloni, "Preliminary study of resistive sensors in inkjet technology for force measurements in biomedical applications," in *Proc. IEEE 11th Int. Multi-Conf. Syst., Signals Devices (SSD)*, Feb. 2014, pp. 1–4.

[65] L. Wang *et al.*, "Design and experiment of a jetting dispenser with compact amplifying mechanism and low stress in piezostack," *J. Intell. Mater. Syst. Struct.*, vol. 31, no. 5, pp. 788–798, Mar. 2020.

[66] J. Fröhlich, D. Gräf, J. Franke, J. Hörber, and M. Hedges, "Customizable capacitive sensor system using printed electronics on window glass," in *Proc. Pan Pacific Microelectron. Symp. (Pan Pacific)*, 2020, pp. 1–6, doi: 10.23919/PanPacific48324.2020.9059446.

[67] N. Ischdonat, C. Dreyer, D. Gräf, J. Franke, J. Hörber, and M. Hedges, "Influences of manufacturing sequences for the application of printed electronics on aircraft interior components," in *Proc. 13th Int. Congr. Molded Interconnect Devices (MID)*, 2018, pp. 1–5, doi: 10.1109/ICMID.2018.8526932.

[68] N. J. Wilkinson, M. A. A. Smith, R. W. Kay, and R. A. Harris, "A review of aerosol jet printing—A non-traditional hybrid process for micro-manufacturing," *Int. J. Adv. Manuf. Technol.*, vol. 105, no. 11, pp. 4599–4619, Dec. 2019.

[69] J. M. Hoey, A. Lutfurakhmanov, D. L. Schulz, and I. S. Akhatov, "A review on aerosol-based direct-write and its applications for microelectronics," *J. Nanotechnol.*, vol. 2012, pp. 1–22, Jun. 2012.

[70] W.-K. Chen, J.-C. Huang, Y.-C. Chen, M.-T. Lee, and J.-Y. Juang, "Deposition of highly transparent and conductive Ga-doped zinc oxide films on tilted substrates by atmospheric pressure plasma jet," *J. Alloys Compounds*, vol. 802, pp. 458–466, Sep. 2019.

[71] P. Sopeña, J. Sieiro, J. M. Fernández-Pradas, J. M. López-Villegas, and P. Serra, "Laser-induced forward transfer: A digital approach for printing devices on regular paper," *Adv. Mater. Technol.*, vol. 5, no. 6, Jun. 2020, Art. no. 2000080.

[72] A. S. Putra, Q. Q. Jiang, K. K. Tan, S. Huang, and T. H. Lee, "Microdispensing system via the contacting method," *ISA Trans.*, vol. 49, no. 4, pp. 443–446, Oct. 2010.

[73] H. Liu, K. Qiao, X. Sun, Q. Gao, Y. Chang, and H. Xu, "Surface tension—Based ultra-micro precision dispensing method for micro—Scale manufacturing and its key influence factors analysis," *J. Micromech. Microeng.*, vol. 30, no. 12, Oct. 2020, Art. no. 125005.

[74] R. Salary, J. P. Lombardi, M. S. Tootooni, R. Donovan, P. K. Rao, and D. M. Poliks, "*In situ* sensor-based monitoring and computational fluid dynamics (CFD) modeling of aerosol jet printing (AJP) process," in *Proc. ASME 11th Int. Manuf. Sci. Eng. Conf. (MSEC)*, 2016, pp. 1–13.

[75] R. Schramm, T. Reitberger, and J. Franke, "Electrical and mechanical investigations on copper circuit paths coated on fiber-reinforced plastics by atmospheric plasma technology," *J. Microelectron. Electron. Packag.*, vol. 12, no. 1, pp. 61–66, Jan. 2015.

[76] P. Lall, K. Goyal, B. Leever, and S. Miller, "Factors influencing the line consistency of commonly used geometries for additively printed electronics," in *Proc. 18th IEEE Intersociety Conf. Thermal Thermomechanical Phenomena Electron. Syst. (ITherm)*, May 2019, pp. 863–869.

[77] P. Lall, A. Abrol, N. Kothari, B. Leever, and S. Miller, "Effect of print parameters on print consistency of aerosol jet printed electronics," in *Proc. 18th IEEE Intersociety Conf. Thermal Thermomechanical Phenomena Electron. Syst. (ITherm)*, May 2019, pp. 633–642.

[78] P. Lall, N. Kothari, K. Goyal, B. Leever, and S. Miller, "Extended-time process consistency and process-property relationships for flexible additive-printed electronics," in *Proc. Pan Pacific Microelectron. Symp. (Pan Pacific)*, Feb. 2020, pp. 1–16.

[79] M. Smith, Y. S. Choi, C. Boughey, and S. Kar-Narayan, "Controlling and assessing the quality of aerosol jet printed features for large area and flexible electronics," *Flexible Printed Electron.*, vol. 2, no. 1, Feb. 2017, Art. no. 015004.

[80] E. B. Secor, "Principles of aerosol jet printing," *Flexible Printed Electron.*, vol. 3, no. 3, Jul. 2018, Art. no. 035002.

[81] G. Chen, Y. Gu, H. Tsang, D. R. Hines, and S. Das, "The effect of droplet sizes on overspray in aerosol-jet printing," *Adv. Eng. Mater.*, vol. 20, no. 8, Aug. 2018, Art. no. 1701084.

[82] K. Lomakin *et al.*, "Evaluation and characterization of 3-D printed pyramid horn antennas utilizing different deposition techniques for conductive material," *IEEE Trans. Compon. Packag. Technol.*, vol. 8, no. 11, pp. 1998–2006, Nov. 2018.

[83] A. Kurz, J. Bauer, and M. Wagner, "Piezo-plunger jetting technology: An experimental study on jetting characteristics of filled epoxy polymers," *Fluids*, vol. 4, no. 1, p. 23, Feb. 2019.

[84] A. Shen, S. B. Kim, C. Bailey, A. W. K. Ma, and S. Dardona, "Direct write fabrication of platinum-based thick-film resistive temperature detectors," *IEEE Sensors J.*, vol. 18, no. 22, pp. 9105–9111, Nov. 2018.

[85] R. Salary, J. P. Lombardi, P. K. Rao, and M. D. Poliks, "Online monitoring of functional electrical properties in aerosol jet printing additive manufacturing process using shape-from-shading image analysis," *J. Manuf. Sci. Eng.*, vol. 139, no. 10, Oct. 2017, Art. no. 101010. Accessed: Aug. 24, 2017.

[86] G. Hu *et al.*, "Functional inks and printing of two-dimensional materials," *Chem. Soc. Rev.*, vol. 47, no. 9, pp. 3265–3300, May 2018.

[87] S. Arakane, M. Mizoshiri, J. Sakurai, and S. Hata, "Three-dimensional Cu microfabrication using femtosecond laser-induced reduction of CuO nanoparticles," *Appl. Phys. Exp.*, vol. 10, no. 1, Jan. 2017, Art. no. 017201.

[88] Y. Sui, L. P. Kreider, K. M. Bogie, and C. A. Zorman, "Fabrication of a silver-based thermistor on flexible, temperature-sensitive substrates using a low-temperature inkjet printing technique," *IEEE Sensors Lett.*, vol. 3, no. 2, pp. 1–4, Feb. 2019.

[89] M. Serpelloni, E. Cantù, M. Borghetti, and E. Sardini, "Printed smart devices on cellulose-based materials by means of aerosol-jet printing and photonic curing," *Sensors*, vol. 20, no. 3, p. 841, Feb. 2020.

[90] C. R. Mejias-Morillo, A. Gbaguidi, D. W. Kim, S. Namilae, and E. A. Rojas-Nastrucci, "UHF RFID-based additively manufactured passive wireless sensor for detecting micrometeoroid and orbital debris impacts," in *Proc. IEEE Int. Conf. Wireless Space Extreme Environ. (WiSEE)*, Oct. 2019, pp. 41–47.

[91] S. Agarwala *et al.*, "Wearable bandage-based strain sensor for home healthcare: Combining 3D aerosol jet printing and laser sintering," *ACS Sensors*, vol. 4, no. 1, pp. 218–226, Jan. 2019.

[92] Z. Pu, Y. Chen, L. Zhang, L. Wang, and Q. Zhang, "Preparation of water soluble acrylic resin adhesive for fluorescent lamps and its modification," *Rare Met.*, vol. 30, no. S1, pp. 657–660, Nov. 2011.

[93] V. Ambardekar, P. P. Bandyopadhyay, and S. B. Majumder, "Atmospheric plasma sprayed SnO_2 coating for ethanol detection," *J. Alloys Compounds*, vol. 752, pp. 440–447, Jul. 2018.

[94] V. Ambardekar, P. P. Bandyopadhyay, and S. B. Majumder, "Hydrogen sensing performance of atmospheric plasma sprayed tin dioxide coating," *Int. J. Hydrogen Energy*, vol. 44, no. 26, pp. 14092–14104, May 2019.

[95] H. Huang *et al.*, "Graphene-based sensors for human health monitoring," *Frontiers Chem.*, vol. 7, p. 399, Jun. 2019.

[96] Z. Yang *et al.*, "Graphene textile strain sensor with negative resistance variation for human motion detection," *ACS Nano*, vol. 12, no. 9, pp. 9134–9141, Sep. 2018.

[97] F. R. Geisenhof *et al.*, "Quantum anomalous Hall octet driven by orbital magnetism in bilayer graphene," *Nature*, vol. 598, no. 7879, pp. 53–58, Oct. 2021.

[98] X. Zhan, C. Si, J. Zhou, and Z. Sun, "MXene and MXene-based composites: Synthesis, properties and environment-related applications," *Nanosc. Horizons*, vol. 5, no. 2, pp. 235–258, Feb. 2020.

[99] A. Sinha *et al.*, "MXene: An emerging material for sensing and biosensing," *TrAC Trends Anal. Chem.*, vol. 105, pp. 424–435, Aug. 2018.

[100] M. Saeidi-Javash *et al.*, "All-printed MXene–graphene nanosheet-based bimodal sensors for simultaneous strain and temperature sensing," *ACS Appl. Electron. Mater.*, vol. 3, no. 5, pp. 2341–2348, May 2021.

[101] A. Li, A. E. Bogdanovich, and P. D. Bradford, "Aligned carbon nanotube sheet piezoresistive strain sensors," *Smart Mater. Struct.*, vol. 24, no. 9, Jul. 2015, Art. no. 095004.

[102] L. Wang and Y. Li, "A review for conductive polymer piezoresistive composites and a development of a compliant pressure transducer," *IEEE Trans. Instrum. Meas.*, vol. 62, no. 2, pp. 495–502, Feb. 2013.

[103] L. Wang, D. Lv, and F. Wang, "Electrode-shared differential configuration for pressure sensor made of carbon nanotube-filled silicone rubber composites," *IEEE Trans. Instrum. Meas.*, vol. 67, no. 6, pp. 1417–1424, Jun. 2018.

[104] E. G. Bakhoum and M. H. M. Cheng, "Miniature carbon monoxide detector based on nanotechnology," *IEEE Trans. Instrum. Meas.*, vol. 62, no. 1, pp. 240–245, Jan. 2013.

[105] Y.-N. Zhangd, E. Siyu, B. Tao, Q. Wu, and B. Han, "Reflective SPR sensor for simultaneous measurement of nitrate concentration and temperature," *IEEE Trans. Instrum. Meas.*, vol. 68, no. 11, pp. 4566–4574, Nov. 2019.

[106] L. Wang, "Potential of using coil-shaped conductive polymer composite to measure temperature and noncontact gap," *IEEE Trans. Instrum. Meas.*, vol. 70, pp. 1–6, 2021.

[107] *Aerosol Jet R Printed Electronics Overview*, Optomec, Albuquerque, NM, USA, 2014, pp. 1–6.

[108] N. G. Di Novo, E. Cantù, S. Tonello, E. Sardini, and M. Serpelloni, "Support-material-free microfluidics on an electrochemical sensors platform by aerosol jet printing," *Sensors*, vol. 19, no. 8, p. 1842, Apr. 2019.

[109] B. Ando, S. Baglio, C. O. Lombardo, V. Marletta, and A. Pistorio, "A low-cost accelerometer developed by inkjet printing technology," *IEEE Trans. Instrum. Meas.*, vol. 65, no. 5, pp. 1242–1248, May 2016.

[110] L. Nayak, S. Mohanty, S. K. Nayak, and A. Ramadoss, "A review on inkjet printing of nanoparticle inks for flexible electronics," *J. Mater. Chem. C*, vol. 7, no. 29, pp. 8771–8795, 2019.

[111] D.-H. Lee, S.-Y. Han, G. S. Herman, and C.-H. Chang, "Inkjet printed high-mobility indium zinc tin oxide thin film transistors," *J. Mater. Chem.*, vol. 19, pp. 3135–3137, Apr. 2009.

[112] P. Aminayi, B. R. Young, T. L. Young, L. H. Sprowl, and M. K. Joyce, "Inkjet printing and surface treatment of an optimized polyurethane-based ink formulation as a suitable insulator over silver for contact with aqueous-based fluids in low-voltage applications," *J. Coatings Technol. Res.*, vol. 14, no. 3, pp. 641–649, May 2017.

[113] D. J. Hayes, P. W. Cooley, and D. B. Wallace, "Miniature chemical and biomedical sensors enabled by direct-write microdispensing technology," *Chem. Biol. Sens. V*, vol. 5416, p. 73, Aug. 2004.

[114] B. Weng *et al.*, "Wholly printed polypyrrole nanoparticle-based biosensors on flexible substrate," *J. Mater. Chem. B*, vol. 2, no. 7, pp. 793–799, 2014.

[115] X. Li, J. Tian, G. Garnier, and W. Shen, "Fabrication of paper-based microfluidic sensors by printing," *Colloids Surf. B, Biointerfaces*, vol. 76, no. 2, pp. 564–570, Apr. 2010.

[116] D. H. Olson *et al.*, "Evolution of microstructure and thermal conductivity of multifunctional environmental barrier coating systems," *Mater. Today Phys.*, vol. 17, Mar. 2021, Art. no. 100304.

[117] G. Mauer, M. O. Jarligo, D. Marcano, S. Rezanka, D. Zhou, and R. Vasen, "Recent developments in plasma spray processes for applications in energy technology," in *Proc. IOP Conf. Mater. Sci. Eng.*, vol. 181, no. 1, Mar. 2017, Art. no. 012001.

[118] W. Ma, W. X. Pan, and C. K. Wu, "Preliminary investigations on low-pressure laminar plasma spray processing," *Surf. Coatings Technol.*, vol. 191, nos. 2–3, pp. 166–174, Feb. 2005.

[119] H. W. Tan, J. An, C. K. Chua, and T. Tran, "Metallic nanoparticle inks for 3D printing of electronics," *Adv. Electron. Mater.*, vol. 5, no. 5, May 2019, Art. no. 1800831.

[120] S. Saxena and J. Jang, "Protrusions of super grains formed by ultrashort Xe flash-lamp annealing of amorphous silicon and its effect on the performances of thin-film transistors," *IEEE Trans. Electron Devices*, vol. 58, no. 8, pp. 2638–2643, Aug. 2011.

[121] F. Ootsuka *et al.*, "Ultralow-thermal-budget CMOS process using flash-lamp annealing for 45 nm metal/high-*k* FETs," *IEEE Trans. Electron Devices*, vol. 55, no. 4, pp. 1042–1049, Apr. 2008.

[122] K.-H. Jung, J. Kim, B.-G. Park, C.-J. Lee, H.-J. Sung, and S.-B. Jung, "Fabrication of ag circuit embedded in PDMS substrate and its mechanical and electrical property with variations of photonic energy," *J. Alloys Compounds*, vol. 748, pp. 898–904, Jun. 2018.

[123] P. Lall *et al.*, "Effect of sintering time and sintering temperature on the mechanical and electrical properties of aerosol-jet additively printed electronics," in *Proc. 18th IEEE Intersociety Conf. Thermal Thermomechanical Phenomena Electron. Syst. (ITherm)*, May 2019, pp. 956–964.

[124] M. Borghetti, E. Cantu, E. Sardini, M. Serpelloni, and A. Ponzoni, "Preliminary analysis on a paper-based ammonia sensor for future food smart packaging," in *Proc. IEEE Int. Workshop Metrology Ind. IoT (MetroInd&IoT)*, Jun. 2021, pp. 140–144.

[125] V. Selamneni, S. K. Ganeshan, N. Nerurkar, T. Akshaya, and P. Sahatiya, "Facile fabrication of $MoSe_2$ on paper as an electromechanical piezoresistive pressure–strain sensor," *IEEE Trans. Instrum. Meas.*, vol. 70, pp. 1–8, 2021.

[126] G. Di Pasquale, S. Graziani, A. Pollicino, and C. Trigona, "Performance characterization of a biodegradable deformation sensor based on bacterial cellulose," *IEEE Trans. Instrum. Meas.*, vol. 69, no. 5, pp. 2561–2569, May 2020.

[127] M. S. Komlenok *et al.*, "Printing of crumpled CVD graphene via blister-based laser-induced forward transfer," *Nanomaterials*, vol. 10, no. 6, p. 1103, Jun. 2020.

[128] V. S. Turkani *et al.*, "Nickel based printed resistance temperature detector on flexible polyimide substrate," in *Proc. IEEE SENSORS*, Oct. 2018, pp. 1–4.

[129] K. N. Paracha, S. K. A. Rahim, H. T. Chattha, S. S. Aljaafreh, S. U. Rehman, and Y. C. Lo, "Low-cost printed flexible antenna by using an office printer for conformal applications," *Int. J. Antennas Propag.*, vol. 2018, pp. 1–7, Feb. 2018.

[130] M. Borghetti, T. Fapanni, N. F. Lopomo, E. Sardini, and M. Serpelloni, "A preliminary study on aerosol jet-printed stretchable dry electrode for electromyography," in *Applications in Electronics Pervading Industry, Environment and Society* (Lecture Notes in Electrical Engineering), vol. 738. Nov. 2020, pp. 292–296.

[131] S. Tonello *et al.*, "Ink-jet printed stretchable sensors for cell monitoring under mechanical stimuli: A feasibility study," *J. Mech. Med. Biol.*, vol. 19, no. 6, Sep. 2019, Art. no. 1950049, doi: 10.1142/S0219519419500490.

[132] S. Chung, K. Cho, and T. Lee, "Recent progress in inkjet-printed thin-film transistors," *Adv. Sci.*, vol. 6, no. 6, Mar. 2019, Art. no. 1801445.

[133] P. V. Arsenov, A. A. Efimov, and V. V. Ivanov, "Optimizing aerosol jet printing process of platinum ink for high-resolution conductive microstructures on ceramic and polymer substrates," *Polymers*, vol. 13, no. 6, p. 918, Mar. 2021.

[134] M. T. Rahman and R. Panat, "Aerosol jet 3D printing and high temperature characterization of nickel nanoparticle films," *Manuf. Lett.*, vol. 29, pp. 5–10, Aug. 2021.

[135] P. Lall, K. Goyal, K. Schulze, and C. Hill, "Print-consistency and process-interaction for inkjet-printed copper on flexible substrate," in *Proc. ASME Int. Tech. Conf. Exhib. Packag. Integr. Electron. Photonic Microsystems*, Oct. 2021, Paper V001T03A003.

[136] C. Wang, G.-Y. Hong, K.-M. Li, and H.-T. Young, "A miniaturized nickel oxide thermistor via aerosol jet technology," *Sensors*, vol. 17, no. 11, p. 2602, Nov. 2017.

[137] M. T. Rahman *et al.*, "High performance flexible temperature sensors via nanoparticle printing," *ACS Appl. Nano Mater.*, vol. 2, no. 5, pp. 3280–3291, May 2019.

[138] M. Borghetti, M. Serpelloni, and E. Sardini, "Printed strain gauge on 3D and low-melting point plastic surface by aerosol jet printing and photonic curing," *Sensors*, vol. 19, no. 19, p. 4220, Sep. 2019.

[139] Y. Han and W. F. Lu, "Structural design of wearable electronics suitable for highly-stretched joint areas," *Smart Mater. Struct.*, vol. 27, no. 10, Oct. 2018, Art. no. 105042.

[140] M. Borghetti, M. Ghittorelli, E. Sardini, M. Serpelloni, and F. Torricelli, "Electrical characterization of PEDOT: PSS strips deposited by inkjet printing on plastic foil for sensor manufacturing," *IEEE Trans. Instrum. Meas.*, vol. 65, no. 9, pp. 2137–2144, Sep. 2016.

[141] C. Zlebic, L. Zivanov, A. Menicanin, N. Blaz, and M. Damnjanovic, "Inkjet printed resistive strain gages on flexible substrates," *Facta Univ. Electron. Energetics*, vol. 29, no. 1, pp. 89–100, 2016.

Paolo Bellitti received the M.Sc. degree in electronic engineering and the Ph.D. degree in technology for health from the University of Brescia, Brescia, Italy, in 2016 and 2019, respectively.

He is currently a Research Fellow with the Department of Information Engineering, University of Brescia. His research activity is mainly focused on the realization of sensors for industrial and biomedical applications obtained both by designing innovative transducers, also through digital and 3-D printing techniques, and by integrating commercial devices to obtain smart objects able to perceive and elaborate environmental parameters.

Michela Borghetti (Member, IEEE) received the master's degree (*cum laude*) in electronic engineering from the University of Brescia, Brescia, Italy, in 2012, the Ph.D. degree from the Universitat Politècnica de Catalunya, Barcelona, Spain, in 2015, and the Ph.D. degree in technology for health from the University of Brescia, in 2016.

She is currently a Post-Doctoral Researcher with the Department of Information Engineering, University of Brescia. She is working on the design and fabrication of sensors for healthcare using low-cost technologies.

Edoardo Cantù (Graduate Student Member, IEEE) received the M.Sc. degree in mechanical engineering—biomechanics curriculum, and the Ph.D. degree in technology for health from the University of Brescia, Brescia, Italy, in 2018 and 2022, respectively.

He is currently a Post-Doctoral Fellow with the Department of Information Engineering, University of Brescia. His research interests deal with design, manufacturing, and testing of sensors and circuits through printed electronics techniques for healthcare sector.

Emilio Sardini (Member, IEEE) received the M.Sc. degree in electronics engineering from the Politecnico di Milano, Milan, Italy, in 1983.

He was a member of the Academic Senate, Board of Directors, University of Brescia, Brescia, Italy, the Deputy Dean of the Engineering Faculty, the Director of the Department of Information Engineering, and a Coordinator of the "Technology for Health" Ph.D. Program. He is currently a Full Professor with the Department of Information Engineering, University of Brescia. His research interests include electronic instrumentation, sensors and signal conditioning electronics, and the development of autonomous sensors for biomedical applications.

Mauro Serpelloni (Senior Member, IEEE) received the M.S. *(cum laude*) degree in industrial management engineering and the Ph.D. degree in electronic instrumentation from the University of Brescia, Brescia, Italy, in 2003 and 2007, respectively.

He is currently a Full Professor with the Department of Information Engineering, University of Brescia. His current research interests include biomechatronic systems, contactless transmission, and signal processing for microelectromechanical systems.